1 **A high-affinity antibody against the CSP N-terminal domain lacks *Plasmodium falciparum***

2 **inhibitory activity**

3

4 **Authors:**

5 Elaine Thai[1,2*], Giulia Costa[3*], Anna Weyrich[3*], Rajagopal Murugan[4], David Oyen[5], Katherine

6 Prieto[2], Alexandre Bosch[2], Angelo Valleriani[3,6], Nicholas C. Wu[5], Tossapol Pholcharee[5], Stephen

7 W. Scally[1], Ian A. Wilson[5,7], Hedda Wardemann[4†], Jean-Philippe Julien[1,2,8†], Elena A. Levashina[3†]

8

9 **Affiliations:**

10 [1]Program in Molecular Medicine, The Hospital for Sick Children Research Institute, Toronto, ON,

11 M5G 1X8, Canada

12 [2]Department of Biochemistry, University of Toronto, ON, M5G 0A4, Canada

13 [3]Vector Biology Unit, Max Planck Institute for Infection Biology, Berlin 10117, Germany

14 [4]B Cell Immunology, German Cancer Research Institute (DKFZ), Heidelberg 69120, Germany

15 [5]Department of Integrative Structural and Computational Biology, The Scripps Research Institute,

16 La Jolla, CA, 92037, United States of America

17 [6]Department of Theory and Biosystems, Max Planck Institute of Colloids and Interfaces, Potsdam

18 14476, Germany

19 [7]The Skaggs Institute for Chemical Biology, The Scripps Research Institute, La Jolla, CA, 92037,

20 United States of America

21 [8]Department of Immunology, University of Toronto, ON, M5G 0A4, Canada

22

23 *These authors contributed equally.

24   †To whom correspondence should be addressed:

25

26   Elena Levashina

27   Vector Biology Unit

28   Max Planck Institute for Infection Biology

29   Campus Charité Mitte

30   Charitéplatz 1

31   10117 Berlin, Germany

32   Tel: +49 30 28460 223

33   levashina@mpiib-berlin.mpg.de

34

35   Jean-Philippe Julien

36   The Hospital for Sick Children Research Institute

37   Peter Gilgan Centre for Research and Learning (PGCRL), Room 20-9703

38   686 Bay St. Toronto ON Canada M5G 0A4

39   Tel: 416-813-7654 ext.309424

40   jean-philippe.julien@sickkids.ca

41

42   Hedda Wardemann

43   B Cell Immunology (D130)

44   Deutsches Krebsforschungszentrum

45   Im Neuenheimer Feld 280

46   69120 Heidelberg, Germany

47   Tel: +49 6221 42 1270

48   h.wardemann@dkfz.de

49

50

51

52   **Abstract**

53   Malaria is a global health concern and research efforts are ongoing to develop a superior vaccine

54   to RTS,S/AS01. To guide immunogen design, we seek a comprehensive understanding of the

55   protective humoral response against *Plasmodium falciparum* circumsporozoite protein (PfCSP).

56   In contrast to the well-studied responses to the repeat region and the C-terminus, the antibody

57   response against the N-terminal domain of PfCSP (N-CSP) remains obscure. Here, we

58   characterized the molecular recognition and functional efficacy of the N-CSP-specific monoclonal

59   antibody 5D5. The crystal structure at 1.85 Å resolution revealed that 5D5 binds an α-helical

60   epitope in N-CSP with high affinity through extensive shape and charge complementarity, and the

61   unusual utilization of an N-linked glycan. Nevertheless, functional studies indicated low 5D5

62   binding to live Pf sporozoites, and lack of sporozoite inhibition *in vitro* and in mosquitoes. Overall,

63   our data on low recognition and inhibition of sporozoites do not support the inclusion of the 5D5

64   epitope into the next generation of CSP-based vaccines.

65   **Summary Statement**

66   The *Plasmodium falciparum* sporozoite surface protein, PfCSP, is an attractive vaccine target, but

67   the antibody response against the CSP N-terminal domain has remained understudied. Here, to

68   guide immunogen design, Thai et al. provide insights into the binding motif and functional efficacy

69   of the N-terminal domain-specific monoclonal antibody, 5D5.

70   **Introduction**

71   Malaria is a vector-borne disease of global importance. In 2017, an estimated 219 million

72   cases were reported, resulting in 435,000 deaths (WHO, 2018). The majority of deaths are caused

73   by *Plasmodium falciparum* (Pf), making this parasite a central focus of research efforts for the

74   development of effective therapeutic interventions. Anti-infection vaccines target the sporozoite

75   stage of the Pf life cycle as parasites are transmitted to the human host by infected female

76   *Anopheles* mosquitos during a blood meal. It has been established four decades ago that mAbs

77   targeting the sporozoite surface circumsporozoite protein (CSP) are capable of neutralizing

78   *Plasmodium* infection (Potocnjak et al., 1980; Yoshida et al., 1980; Yoshida et al., 1981; Cochrane

79   et al., 1982). This year, the current leading anti-infection CSP-based vaccine against Pf malaria,

80   RTS,S/AS01, has begun pilot implementation in Ghana, Malawi and Kenya. Notwithstanding,

81   RTS,S/AS01 has shown to only provide rapidly waning protection in 50% of children and thus,

82   intense research efforts are underway towards designing a more efficacious and durable anti-CSP

83   vaccine (RTS,S Clinical Trials Partnership, 2015; Julien and Wardemann, 2019).

84   A molecular understanding of how the most potent monoclonal antibodies (mAbs)

85   recognize sites of vulnerability on the parasite can guide next-generation vaccine design. PfCSP is

86   composed of an N-terminal domain (N-CSP), a central repeat region comprising NANP motifs of

87   varied number that are interspersed with related NVDP motifs, and a C-terminal domain (C-CSP)

88   that comprises a linker region preceding an α-thrombospondin type-1 repeat (αTSR) domain (Fig.

89   1A). PfCSP is linked to the parasite membrane through a glycosylphosphatidylinositol anchor site.

90   Numerous studies have shown that mAbs specific for the NANP repeat region and the junction

91   immediately following N-CSP, which contains NANP motifs, NVDV motifs and the only copy of

92   an NPDP motif, can mediate protection in animal models (Potocnjak et al., 1980; Yoshida et al.,

5

93   1980; Foquet et al., 2014; Oyen et al., 2017; Triller et al., 2017; Kisalu et al., 2018; Tan et al.,

94   2018; Imkeller et al., 2018; Murugan et al., 2019). The few described mAbs to C-CSP were

95   functionally ineffective, probably, due to low accessibility of this domain on the sporozoite surface

96   (Scally et al., 2018). In contrast, the functional relevance of N-CSP mAbs remains elusive. To

97   date, no human mAb specific for this domain and only a handful of murine mAbs from

98   immunization studies with recombinant Pf N-CSP have been reported (Espinosa et al., 2015;

99   Herrera et al., 2015). These mAbs recognized N-CSP epitopes adjacent to Region I (RI; Fig. 1A),

100   a site with high conservation across *Plasmodium* species, suggesting that RI may be a good target

101   for cross-species vaccine development (Dame et al, 1984; Espinosa et al., 2015). Additionally,

102   proteolytic cleavage of RI was linked to efficient sporozoite invasion of host hepatocytes (Espinosa

103   et al., 2015; Coppi et al., 2005). Based on these observations, it has been proposed that adding N-

104   CSP, including the RI motif, into a PfCSP subunit vaccine may improve protective efficacy

105   compared to the current leading vaccine RTS,S/AS01, which lacks this domain. However, passive

106   transfer of the most potent RI-targeting mAb 5D5 protected mice from infection in only one of the

107   two tested transgenic rodent *P. berghei* (Pb) models that expressed a chimeric PbCSP with the Pf

108   N-CSP domain (Espinosa et al., 2015), and its impact on Pf has not been determined. Thus, crucial

109   information on how mAb 5D5 binds and inhibits Pf sporozoites is still missing.

110   To gain a molecular understanding of how the mAb 5D5 recognizes PfCSP and inhibits Pf

111   sporozoite infectivity, we solved the crystal structure of the 5D5 Fab in complex with a peptide

112   derived from N-CSP and conducted in-depth binding and functional experiments with Pf

113   sporozoites. We specifically quantified reactivity of mAb 5D5 to single live Pf sporozoites isolated

114   from the midgut and salivary glands of mosquitoes using imaging flow cytometry, and tested its

115   inhibitory potency against Pf sporozoites through *in vitro* traversal assays and *in vivo* passive mAb

116   transfer experiments in mosquitoes. Our work provides a detailed molecular and functional

117   understanding of mAb 5D5 recognition of its epitope, and highlights poor recognition of this N-

118   CSP epitope on the Pf sporozoite surface.

119

120   **Results and Discussion**

121   **mAb 5D5 binds an α-helical motif in N-CSP**

122   To understand the molecular basis for mAb 5D5 recognition of PfCSP, we solved the

123   crystal structure of the 5D5 Fab in complex with PfCSP$_{81-98}$ to 1.85 Å resolution (Supplementary

124   Table 1). We specifically selected PfCSP residues 81-98 for our studies to ensure inclusion of the

125   mAb 5D5 epitope, identified as Pf N-CSP residues 82-91 by yeast display epitope mapping (Fig.

126   1A and S1A) in agreement with previous reports (Espinosa et al., 2015), as well as conserved RI

127   residues KLKQP in positions 93-97. Consistent with our yeast display experiments, we observed

128   strong electron density for N-CSP residues 81-92 (EDNEKLRKPKHK) in the crystal structure

129   (Fig. S1B). PfCSP residues 83-91 formed an α-helix when bound by 5D5 Fab (Fig. 1B), in line

130   with secondary structure predictions based on the primary sequence (Drozdetskiy et al., 2015).

131   Importantly, while structures of a variety of polypeptides derived from PfCSP (the junctional

132   region following N-CSP, the NANP repeat region, and the C-terminal αTSR domain) have been

133   solved in complex with a broad range of antibodies (Oyen et al., 2017; Imkeller et al., 2018; Scally

134   et al., 2018; Tan et al., 2018; Kisalu et al., 2018; Julien and Wardemann, 2019; Murugan et al.,

135   2019), our crystal structure of the 5D5 Fab in complex with PfCSP$_{81-98}$ provides the first insight

136   into the subdomain architecture of Pf N-CSP. However, further studies are needed to elucidate the

137   conformation of residues comprising RI, which were disordered and unresolved in our crystal

138   structure, as well as the overall structure of Pf N-CSP.

7

139

140
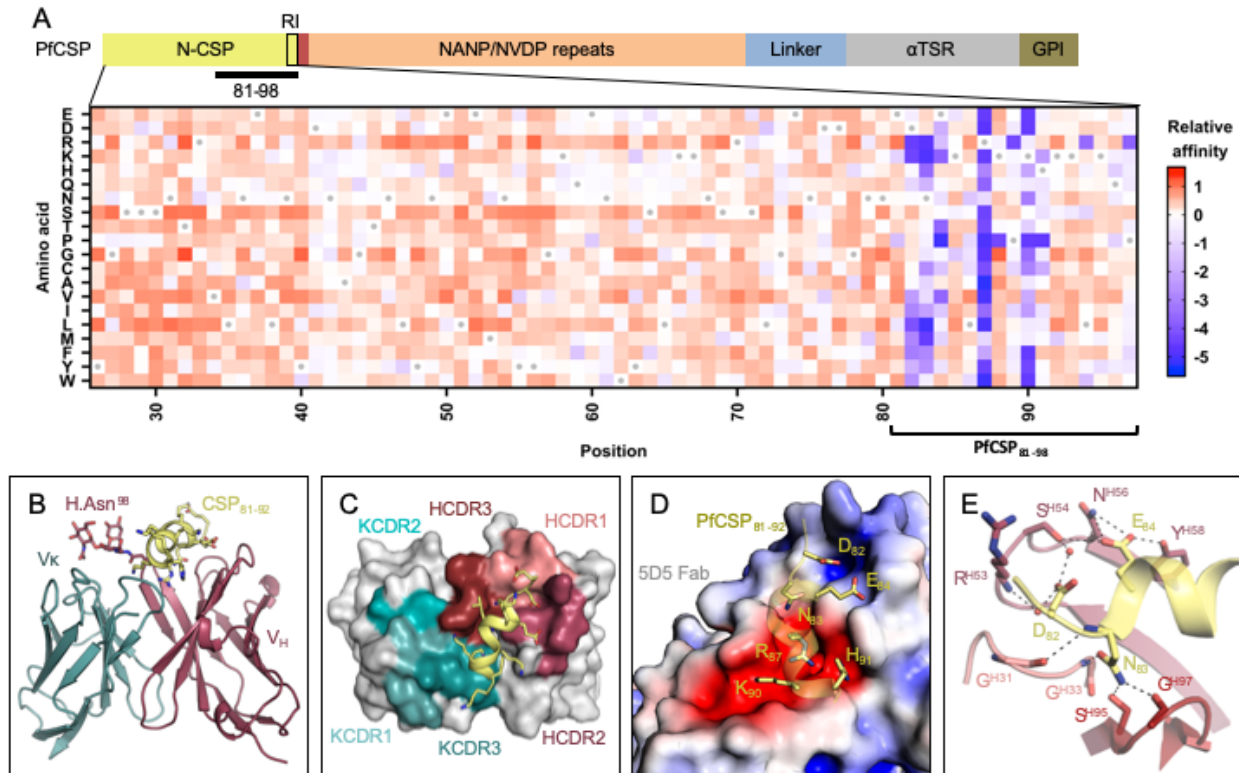
Figure 1. Molecular delineation of the mAb 5D5 epitope in PfCSP. (A, above) Schematic depicting the protein domain organization of PfCSP shown with the approximate location of Region I (RI) indicated by the black box and the junctional epitope represented by a dark red band. An approximate representation of PfCSP$_{81-98}$ is illustrated by the black bar (not shown to scale). (Below) Heatmap of mAb 5D5 binding affinity for N-CSP single point mutant library. N-CSP residues included in PfCSP$_{81-98}$ are indicated by the bracket at the bottom. The relative binding affinity is indicated by a diverging colour scale from red to blue, where red indicates a similar affinity while blue indicates decreased affinity. The X-axis denotes the N-CSP residue position and the Y-axis specifies the introduced single point mutations. Residues corresponding to the WT sequence are indicated by the gray dots. (B) Crystal structure showing the 5D5 Fab variable regions (heavy chain shown in red and kappa light chain shown in blue) bound to PfCSP N-terminal residues 81-92 (yellow), which are recognized in an α-helical conformation. The N-linked glycan on H.Asn98 of 5D5 Fab is represented as sticks. (C) mAb 5D5 CDRs contacting PfCSP. HCDRs 1, 2, and 3 (salmon, raspberry and firebrick red, respectively), and KCDRs 1 and 3 (light teal and deep teal, respectively) contribute to 5D5 Fab recognition, whereas KCDR2 (teal) does not. (D) Electrostatic surface potential of mAb 5D5 bound to PfCSP$_{81-98}$. mAb 5D5 displays extensive shape and charge complementarity to PfCSP. Electrostatic calculations were performed using APBS (Baker et al., 2001) and rendered in Pymol (The PyMOL Molecular Graphics System, Version 2.0 Schrödinger, LLC); scale: -5 kT/e (red) to +5 kT/e (blue). (E) H-bonds (shown as black dashed lines) formed between mAb 5D5 HCDR residues and negatively charged PfCSP residues. Water molecules are shown as red spheres.

8

158   mAb 5D5 contacts PfCSP with all complementarity-determining regions (CDRs) except

159   kappa light chain CDR 2 (KCDR2; Fig. 1C). The heavy chain CDRs (HCDRs) form the majority

160   of interactions with 498 $Å^2$ buried surface area (BSA) compared to 160 $Å^2$ BSA for the kappa light

161   chain. Furthermore, the mAb 5D5 CDRs possess extensive shape and electrostatic

162   complementarity to this highly charged N-CSP epitope (Fig. 1D). An electropositive pocket

163   formed by HCDR2 contacts PfCSP residues D82 and E84 via H-bonds with Ser54$^{O\gamma}$, Asn56$^{N\delta2}$,

164   and Tyr58^{OH}, and water-mediated H-bonds with Arg53^N and Ser54$^{O\gamma}$ (Fig. 1E). Additionally, an

165   electronegative pocket formed by HCDR2, HCDR3, KCDR1, and KCDR3 contacts PfCSP

166   electropositive residues R87, K90 and H91 via several H-bonds and salt bridges (Fig. 2A). The

167   significance of this shape and charge complementarity for high affinity binding was observed in

168   our yeast display experiments, as mutations maintaining both side chain length and electrostatic

169   properties, such as K90R, were more likely to sustain high affinity binding than those that did not

170   (K90E, K90D; Fig. 1A).

171   Consistent with prediction from the primary mAb 5D5 sequence, we observed electron

172   density for two GlcNAc and one α1-6Fuc moieties indicative of N-linked glycosylation at Asn98

173   of HCDR3 (Fig. 2A and S1C). Importantly, the first N-linked GlcNAc moiety contacts the

174   aliphatic portion of K90 of PfCSP$_{81-98}$, conferring 48 $Å^2$ of BSA, while the other sugars did not

175   interact with the peptide. In this way, the paratope glycan contributes to mAb 5D5 occlusion of

176   PfCSP residue K90. Interestingly, K90 is one of four lysine residues (including K85, K88, and

177   K92) directly upstream of RI that have previously been proposed to be important for binding

178   heparan sulfate proteoglycans on the surface of hepatocytes to initialize liver invasion (Zhao et al.,

179   2016). Notably, the α-helical conformation adopted by N-CSP residues 83-91 upon mAb 5D5

180   binding positions the remaining three lysine residues, K85, K88 and K92, on the same exposed

181   face of the helix (Fig. S1B). Thus, our molecular description of PfCSP recognition by mAb 5D5

182   demonstrates optimal antibody-antigen characteristics associated with high affinity binding to a

183   putative functional site on Pf sporozoites.

184

185   **mAb 5D5 paratope glycosylation is critical for high affinity recognition of recombinant**

186   **PfCSP**

187   To determine whether the N-linked glycan on H.Asn98 affects mAb 5D5 binding, we

188   generated four different forms of the mAb 5D5 glycan and measured their binding kinetics to full-

189   length PfCSP using biolayer interferometry (BLI; Fig. 2B-F). Specifically, we generated four 5D5

190   Fab variants with either: 1) a complex glycan, as in the crystal structure (by expression in HEK

191   293F cells; 293F); 2) a high mannose glycan (by expression in HEK 293S (GnT I$^{-/-}$) cells; 293S

192   (GnT I$^{-/-}$)); 3) a single GlcNAc moiety (by expression in HEK 293S (GnT I$^{-/-}$) cells followed by

193   Endo H treatment; Endo H); or 4) an H.N98Q mutation removing the N-linked glycosylation site

194   altogether (5D5Δg). The 293F, 293S (GnT I$^{-/-}$) and Endo H-treated 5D5 Fabs bound with high

195   affinity to full-length PfCSP with K_D's of 39.7 ± 8.2 nM, 46.6 ± 4.7 nM and 85.8 ± 8.8 nM,

196   respectively (Fig. 2C-E). In contrast, the 5D5Δg mutant Fab bound PfCSP with weaker affinity

197   (K_D of 453 ± 110 nM) due to an 11-fold faster off-rate compared to HEK 293F-expressed 5D5 Fab

198   (Fig. 2B and F), while the on-rates of all glycoform Fabs remained within the same order of

199   magnitude. Together with the crystal structure, these results underline the importance of the

200   H.Asn98-linked GlcNAc moiety for high affinity mAb 5D5 binding to recombinant PfCSP, and

201   highlight a rare occurrence for such a post-translational modification to participate in the antibody-

202   antigen interaction and improve the kinetics of antigen binding.
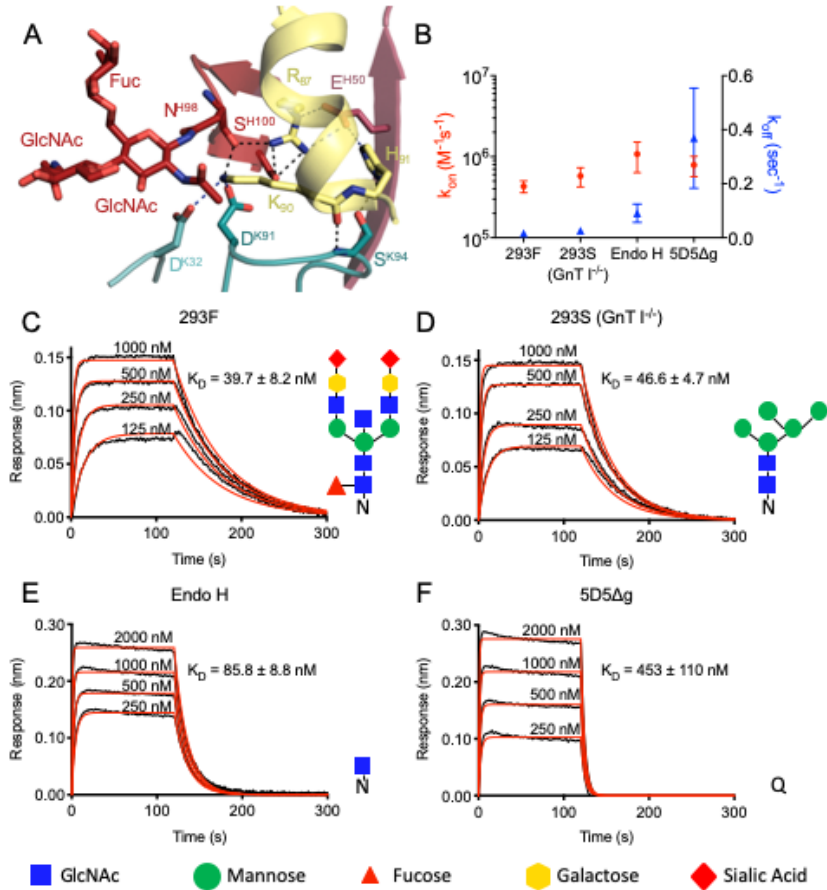
Figure 2. 5D5 paratope glycosylation mediates high affinity binding. (A) Interactions formed by mAb 5D5 H.Asn98-linked GlcNAc moiety and surrounding CDR residues with PfCSP. H-bonds are shown as black dashed lines, and salt bridges are shown as blue dashed lines. (B-F) Binding kinetics of twofold dilutions of (C) 293F, (D) 293S (GnT I$^{-/-}$), (E) Endo H and (F) 5D5Δg Fab glycoform variants to full length PfCSP. (B) Mean k_{on} and k_{off} rates of the 5D5 Fab glycoform variants binding to full length PfCSP are plotted on the left and right y-axis, respectively. Mean k_{on} rates are shown as red circles, and mean k_{off} rates as blue triangles. (C-F) Representative sensorgrams are shown in black and 1:1 model best fits in red. Mean K_D values are as listed. K_D values, and k_{on} and k_{off} rates were determined by FortéBio's Data Analysis software 9.0. Standard error values are reported as the standard deviation. Data are representative of three independent measurements. Corresponding glycan structures are shown using symbols adhering to the Symbol Nomenclature for Glycans (Varki et al., 2015) .

mAb 5D5 does not efficiently bind or inhibit salivary gland Pf sporozoites

The role of the N-linked glycan on H.Asn98 in the binding of 5D5 IgG to freshly isolated salivary gland Pf sporozoites was quantified by imaging flow cytometry. As these preparations

11

218   contained both live and dead sporozoites, we focused our analyses on live sporozoites that were

219   negative for propidium iodide staining (Fig. S2). As positive and negative controls, we used human

220   mAbs targeting the PfCSP central repeat (1210; Imkeller et al., 2018) and C-CSP (1710; Scally et

221   al., 2018), respectively. In line with previous reports, mAb 1710 failed to recognize mature Pf

222   sporozoites isolated from mosquito salivary glands, whereas mAb 1210 strongly bound these

223   sporozoites (Fig. 3A-D). We detected a two-fold decrease in mean fluorescence intensity (MFI)

224   between mAbs 1210- and 5D5- or 5D5Δg-bound sporozoites (Fig. 3C). The observed differences

225   can be explained by the frequencies of the targeted epitopes on the sporozoite surface. Indeed,

226   mAb 1210 likely binds repeated NANP motifs within the central region whereas mAbs 5D5 and

227   5D5Δg can only react with a single N-CSP motif. In contrast to previous reports, we found that

228   mAbs 5D5 did not bind the majority of sporozoites (Fig. 3B and D). Mutation of the glycosylation

229   site further decreased the proportion of 5D5Δg-bound sporozoites from 27 to 13% (Fig. 3D). These

230   results demonstrate the importance of mAb 5D5 paratope glycosylation for PfCSP binding on the

231   sporozoite surface. However, they also reveal low levels of overall reactivity of this antibody to

232   live salivary gland Pf sporozoites.
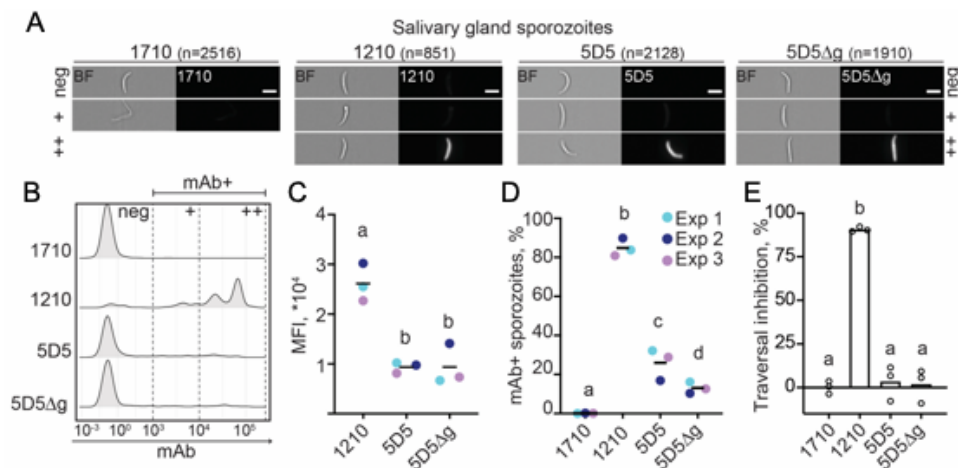
233

234 **Figure 3. mAb 5D5 binding to salivary gland sporozoites and traversal inhibition activity.** (A-D) Imaging flow
235 cytometry of live salivary gland sporozoites isolated from mosquito thorax after incubation with human mAb 1710 or
236 1210 (negative and positive controls, respectively), or mAb 5D5 or 5D5Δg. (A) Representative images of sporozoites
237 in brightfield (BF, left panels) and mAb-bound fluorescent sporozoites (right panels). Scale bars - 5 μm. Total number
238 of sporozoites analysed per condition is indicated in parentheses (N=3). (B) Comparative density plots of a
239 representative experiment showing the fluorescence intensities of three arbitrarily-designated groups of mAb-bound
240 sporozoites (neg – negative, + – low intensity, ++ – high intensity). (C) Mean fluorescence intensities (MFI) of the
241 mAb-positive sporozoites. (D) Quantification of mAb-positive sporozoites (%). (C-D) Colors show results of three
242 independent experiments. (E) Results of mAb inhibition of sporozoites in *in vitro* traversal assay tested at 100 μg/mL
243 mAb concentration (N=3). Statistically significant differences (p<0.05) between the groups are indicated by different
244 letters (z-test (C and D); paired Friedman test followed by Dunn's *post-hoc* test (E)).
245

246   We next evaluated how the low sporozoite binding observed for mAb 5D5 translated into

247 inhibitory potency against Pf sporozoites in a hepatocyte traversal assay. In line with the mAb

248 binding efficiencies, only mAb 1210 completely blocked sporozoite traversal of hepatocytes,

249 whereas mAb 5D5 was as inefficient at inhibiting traversal as negative control mAb 1710,

250 regardless of the presence of the paratope glycan (Fig. 3E). Poor mAb 5D5 binding to sporozoites

251 and lack of traversal inhibition precluded further functional testing of mAb 5D5 in Pf infections in

252 a sophisticated humanized mouse model. We conclude that, in spite of high affinity interaction

253 with the N-CSP epitope in recombinant PfCSP, the overall low levels of mAb 5D5 binding to live

254 Pf sporozoites preclude efficient inhibition of parasite traversal.

255

256 **mAb 5D5 does not inhibit *in vivo* sporozoite development in mosquitoes**

257   As CSP is essential for sporozoite development in mosquitoes (Menard et al., 1997), we

258 extended our antibody binding and functional examination to immature Pf sporozoites isolated

259 from oocysts in the mosquito midgut (Fig. 4A). Similar to our observations with mature

260 sporozoites, mAb 5D5 exhibited low binding efficiency to immature sporozoites, as measured by

261 MFI and percentage of mAb-positive sporozoites determined using imaging flow cytometry (Fig.

13

262   4B-C). Also consistent with our findings with salivary gland sporozoites, paratope glycosylation

263   increased the proportion of mAb 5D5-bound midgut sporozoites by two-fold (Fig. 4D).

264
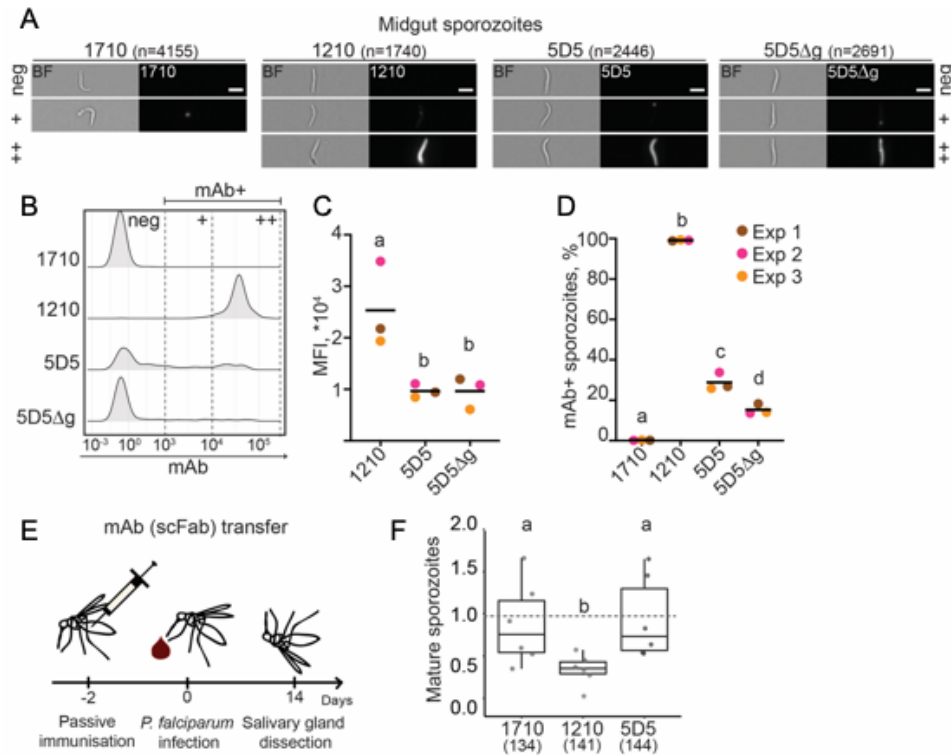
Figure 4. mAb 5D5 binding to midgut sporozoites and inhibition of sporogonic development within mosquitoes.
(A-D) Imaging flow cytometry of live midgut sporozoites isolated from oocysts after incubation with human mAb
1710 or 1210 (negative and positive controls, respectively), or mAb 5D5 or 5D5Δg. (A) Representative images of
sporozoites in brightfield (BF, left panels) and mAb-bound fluorescent sporozoites (right panels). Scale bars - 5 μm.
Total number of sporozoites analysed per condition is indicated in parentheses (N=3). (B) Comparative density plots
of a representative experiment showing the fluorescence intensities of three arbitrarily-designated groups of mAb-
bound sporozoites (neg – negative, + – low intensity, ++ – high intensity). (C) Mean fluorescence intensities (MFI) of
the mAb-positive sporozoites. (D) Quantification of mAb-positive sporozoites (%). (C-D) Colors show results of three
independent experiments. (E) Schematic representation of passive single-chain Fab (scFab) transfer by mosquito
injection. (F) Results of scFab transfer experiments expressed relative to control PBS-injected mosquitoes (N=6, total
mosquito numbers analyzed are indicated below in parentheses). The box plots show the upper and lower quantiles
and the median of the distribution. Each dot represents normalized sporozoite loads in one experiment. Statistically
significant differences (p<0.05) between the groups are indicated by different letters (z-test (C and D); maximum
likelihood estimation (MLE)(F)).

279

14

280   To evaluate the inhibitory activity of mAb 5D5 against Pf sporozoites in their natural

281   environment *in vivo*, we developed a passive mAb transfer assay for mosquitoes that examined

282   sporozoite maturation and salivary gland invasion. Mosquitoes were injected with recombinant

283   single-chain Fabs (scFabs) two days before Pf infection, and sporozoite loads in dissected salivary

284   glands were quantified two weeks later (Fig. 4E). Injection of scFab1210 significantly reduced the

285   number of mature sporozoites in the salivary glands. In contrast, transfer of scFab1710 or

286   scFab5D5 did not affect sporozoite development and invasion (Fig. 4F). Taken together, these

287   results demonstrate that mAb 5D5 fails to efficiently recognize its epitope on the surface of Pf

288   parasites, and lacks inhibitory potency against sporozoites in both the vector and the host.

289

290   **Concluding Remarks**

291   In this report, we demonstrate that despite high-affinity binding to recombinant PfCSP,

292   mAb 5D5 does not recognize the majority of live Pf sporozoites, indicating that its epitope is not

293   readily accessible or present on the sporozoite surface. Consequently, as shown in the current

294   study, mAb 5D5 is unable to block Pf sporozoite development in the mosquito or inhibit sporozoite

295   traversal of hepatocytes. The lack of potent human N-CSP-specific mAbs in multiple screens based

296   on full-length recombinant PfCSP baits or unbiased antigen-agnostic approaches (Fig. S3; Triller

297   et al., 2017; Murugan et al., 2018; Tan et al., 2018; Kisalu et al., 2018; Julien and Wardemann,

298   2019) is in line with these observations. Overall, to date, there is little evidence to support N-CSP

299   as a source of potent or protective epitopes to block Pf infection. Therefore, the repeating motifs

300   in the central domain and N-terminal junction remain the most promising PfCSP regions for anti-

301   infective vaccine design to elicit protective mAbs.

302 **Materials and Methods**

303 **Mutant N-CSP yeast display library construction and transformation**

304   Epitope mapping using phage display was adapted from a previously published method

305 (Van Blarcom et al., 2015). Construction of the mutant library required generation of a linearized

306 vector and a library of mutant N-CSP inserts. The mutant insert library was generated by two

307 rounds of PCR using primers that carried the randomized codon "NNK" (Tables S2 and S3), and

308 mixing the products (Amplicons 1 to 9) at an equal molar ratio. The vector was generated by

309 overlapping PCR using vector-F/R primers (Table S2). All PCR products were amplified using

310 KOD DNA polymerase (EMD Millipore) and purified by gel extraction (Clontech Libraries).

311   The EBY100 yeast strain was purchased from ATCC. The yeast vector was generated by

312 modification of the commercially available pCTcon2 vector (Addgene; Chao et al., 2006). The

313 mutant N-CSP insert was cloned with N-terminal V5 and C-terminal HA epitope tags. The Aga2p

314 yeast protein gene was inserted downstream of the HA epitope tag to allow for yeast surface

315 display of the N-CSP (plasmid pCTcon2-rsCSP-V5-HA-Aga2p). Yeast transformation was

316 performed as described previously (Benatuil et al., 2010). In summary, 4 µg of the linearized yeast

317 expression vector and 8 µg of the N-CSP mutant library insert were used for transformation.

318 Transformants were plated on SDCAA plates and incubated at 30°C for 2 days. Over 10^8 colonies

319 were collected, resuspended in YPD media with 15% glycerol, and stored at -80°C until use.

320 **5D5 Fab production and purification**

321   mAb 5D5 V_L and V_H regions were individually cloned into pcDNA3.4-TOPO expression

322 vectors immediately upstream of human Igκ and Igγ1-C_H1 domains, respectively. The resulting

323 5D5 Fab light and heavy chain vectors were co-transfected into either HEK293F or HEK293S

324 (GnT I$^{-/-}$) cells for transient expression, and purified via KappaSelect affinity chromatography (GE

325 Healthcare), cation exchange chromatography (MonoS, GE Healthcare), and size exclusion

326 chromatography (Superdex 200 Increase 10/300 GL, GE Healthcare). For binding studies, 5D5

327 Fab expressed in HEK293S (GnT I$^{-/-}$) cells was digested with Endoglycosidase H, followed by an

328 additional size exclusion chromatography step (Superdex 200 Increase 10/300 GL, GE

329 Healthcare). Lastly, the 5D5Δg Fab was produced by site-directed mutagenesis of the mAb 5D5

330 V$_H$ region using Accuprime Pfx Supermix (Thermo Fisher Scientific). 5D5Δg Fab was expressed

331 in HEK293F cells and purified by chromatography as described above.

332 **IgG production and purification**

333 For yeast display experiments, mAb 5D5 was produced in ExpiCHO cells as a mouse IgG1

334 with AVI tag for biotinylation. The IgG was then purified using protein G affinity chromatography

335 (HiTrap Protein G HP, GE Healthcare) and size-exclusion chromatography (Superdex 200, GE

336 Healthcare). Biotinylation was performed as previously described (Ekiert et al., 2011).

337 For production of 5D5 and 5D5Δg IgGs for non-yeast display experiments, site-directed

338 mutagenesis was performed using In-Fusion (Takara Bio) on the pcDNA3.4-TOPO vectors

339 encoding the 5D5 Fab heavy chain and 5D5Δg Fab heavy chain sequences to substitute two stop

340 codons with two residues (DK), allowing for expression of the Igγ1-CH2 and Igγ1-CH3 domains.

341 5D5 IgG, 5D5Δg IgG, 1710 IgG (Scally et al., 2018), 1210 IgG (Imkeller et al., 2018), and IgGs

342 elicited by the PfSPZ-CVac Challenge (Mordmüller et al., 2017; Murugan et al., 2018) were

343 transiently expressed in HEK293F cells by co-transfection of paired Ig heavy and light chains, and

344 purified through protein A affinity chromatography (GE Healthcare), followed by size exclusion

345 chromatography (Superdex 200 Increase 10/300 GL, GE Healthcare).

346 **scFab production and purification**

17

347   scFab constructs were designed by cloning paired light and heavy chains, separated by a

348   72-residue linker, into a pcDNA3.4-TOPO expression vector. The resulting constructs were

349   transiently expressed in HEK293F cells, and purified by KappaSelect affinity chromatography

350   (GE Healthcare), followed by size exclusion chromatography (Superdex 200 Increase 10/300 GL,

351   GE Healthcare).

352   **Recombinant PfCSP production and purification**

353   A construct of full-length PfCSP isolated from strain NF54 (UniProt accession no. P19597,

354   residues 20-384) was designed with potential N-linked glycosylation sites mutated to glutamine

355   (Scally et al., 2018). The resulting construct was transiently transfected in HEK293F cells, and

356   purified by HisTrap FF affinity chromatography (GE Healthcare) and size exclusion

357   chromatography (Superdex 200 Increase 10/300 GL, GE Healthcare).

358   A construct encoding PfCSP residues 71-104 was cloned into a pETM-22 vector.

359   Competent BL21(DE3) *E. coli* cells were transformed with the resulting plasmid and cultured to

360   an optical density of approximately 0.6-0.8. Expression of $PfCSP_{71-104}$ was induced using 1 mM

361   isopropyl β-D-1-thiogalactopyranoside (IPTG). Approximately 4 h after induction, cells were

362   lysed by sonication, and purified through HisTrap affinity chromatography (GE Healthcare) and

363   size exclusion chromatography (Superdex 75 10/300 GL, GE Healthcare).

364   **Yeast display epitope mapping**

365   For each sorting round, $\sim 10^9$ yeast cells from the frozen stock were cultured in 250 mL of

366   SDCAA media for 16 h at 27.5°C until an OD of 1.9 was reached. Cells were pelleted, resuspended

367   in 35 mL of SGR-CAA induction media and incubated for 30 h at 18°C until an OD of 1.4 was

368   reached. After harvesting approximately 8 mL of cell culture, the pellet was washed 3 times with

369   PBS and finally resuspended in 5 mL of PBS. Biotinylated 5D5 IgG was incubated with BB515-

18

370   streptavidin at a molar ratio of 1:2 for 20 min. The biotinylated 5D5 IgG-streptavidin BB515

371   complex and Anti-HA PE antibody were added to the 5 mL of resuspended yeast cells with a final

372   concentration of 20 nM for each stain, followed by overnight incubation at 4°C with head-to-head

373   rotation in the dark. Next, cells were washed twice with PBS, resuspended in 5 mL of PBS, and

374   sorted at the TSRI Flow Cytometry Core Facility. Two gates were applied for simultaneous sorting

375   (Fig. S1A): one where binding of 5D5 IgG was completely abrogated (PE only) and one where

376   binding was unaffected (PE and BB515). The second round of sorting saw significant enrichment

377   in either gate.

378   **Deep mutational scanning data analysis**

379   Sequencing data were obtained in FASTQ format and parsed using SeqIO module in

380   BioPython (Cock et al., 2009). After trimming the primers, a paired-end read was then filtered and

381   removed if the corresponding forward and reverse reads were not reverse-complemented. The

382   position of the randomized codon was then identified by the internal barcode. Each mutation was

383   called by comparing individual paired-end reads to the wild type (WT) reference sequence.

384   Frequency of mutation m in sample s was computed as:

385
$$Frequency_{m,s} = \frac{read\ count_{m,s} + 1}{total\ read\ count_s}$$

386   Relative affinity of mutation m was computed as:

387
$$Relative\ affinity_m = \log_{10}\left(\frac{Frequency_{m,round\ 2\ gate\ 1}}{Frequency_{m,round\ 2\ gate\ 2}} \div \frac{Frequency_{WT,round\ 2\ gate\ 1}}{Frequency_{WT,round\ 2\ gate\ 2}}\right)$$

388   The pseudo read count of 1 in the calculation of frequency was to prevent division by zero during

389   the calculation of relative affinity. Relative affinity of WT is 0.

390   Raw sequencing data have been submitted to the NIH Short Read Archive under accession

391   number: BioProject PRJNA578947. Custom python scripts for analyzing the deep mutational

392   scanning data have been deposited to https://github.com/wchnicholas/CSP_Nterm_yeast_display.

Crystallization and structure determination

394   Purified 5D5 Fab and CSP 81-98 peptide (GenScript) were mixed in a 1:5 molar ratio. The

395   5D5 Fab/CSP 81-98 complex was then mixed in a 1:1 ratio with 20% (w/v) PEG 3350, 0.2 M di-

396   ammonium citrate. Crystals appeared after ~20 h, and were cryoprotected in 15% (v/v) ethylene

397   glycol before being flash-frozen in liquid nitrogen. Data were collected at the 08ID-1 beamline at

398   the Canadian Light Source, processed and scaled using XDS (Kabsch, 2010). The structure was

399   determined by molecular replacement using Phaser (McCoy et al., 2007) and a Fab model from

400   our internal database as the search model. Refinement of the structure was performed using

401   phenix.refine (Adams et al., 2010) and iterations of refinement using Coot (Emsley et al., 2010).

402   The crystal structure has been deposited in the Protein Data Bank (PDB ID 6UUD).

BLI binding studies

404   BLI (Octet RED96, FortéBio) experiments were conducted to determine the binding

405   kinetics of the 5D5 Fab glycoform variants to recombinant PfCSP diluted to 10 µg/mL in kinetics

406   buffer (PBS, pH 7.4, 0.01% [w/v] BSA, 0.002% [v/v] Tween-20) was immobilized onto Ni-NTA

407   (NTA) biosensors (FortéBio). After a steady baseline was established, biosensors were dipped into

408   wells containing twofold dilutions of each 5D5 Fab glycoform variant in kinetics buffer. Tips were

409   then immersed back into kinetics buffer for measurement of the dissociation rate. Kinetics data

410   were analyzed using FortéBio's Data Analysis software 9.0, and curves were fitted to a 1:1 binding

411   model. Mean kinetic constants and corresponding standard deviation values are reported as the

412   result of three independent experiments for each 5D5 Fab glycoform variant.

413   BLI experiments were also done to determine the avidity of IgGs isolated from the PfSPZ-

414   CVac Challenge (Mordmüller et al., 2017) to full length recombinant PfCSP and N-CSP construct,

415   PfCSP$_{71-104}$. Unrelated malaria protein Pfs25 was used to block non-specific binding and 5D5 IgG

416   was used as a positive control. PfCSP$_{71-104}$, PfCSP or Pfs25 was diluted to 10 μg/mL in kinetics

417   buffer and immobilized onto Ni-NTA (NTA) biosensors (FortéBio). Once a stable baseline was

418   established, biosensors were dipped into wells, each containing a different IgG diluted to 500 nM

419   in kinetics buffer. Tips were subsequently dipped back into kinetics buffer to observe any

420   dissociation of IgG.

Mosquito rearing, parasite infections and sporozoite isolations

422   *Anopheles coluzzii* (Ngousso strain) mosquitoes were maintained at 29°C 70–80%

423   humidity 12/12 h day/night cycle. For *P. falciparum* infections, mosquitoes were fed for 15 min

424   on a membrane feeder with NF54 gametocytes cultured with O$^+$ human red blood cells (Haema,

425   Berlin), and, thereafter, kept in a secured S3 laboratory according to the national regulations

426   (Landesamt für Gesundheit und Soziales, project number 297/13). The *P. falciparum* NF54 clone

427   used in this study originated from Prof. Sauerwein's laboratory (RUMC, Nijmegen) and was

428   authenticated for *Pfs47* genotype by PCR on genomic DNA. *P. falciparum* asexual cultures were

429   monthly tested for *Mycoplasma* contamination. Unfed mosquitoes were removed shortly after

430   infections. Blood fed mosquitoes were offered an additional uninfected blood meal eight days post

431   infection, maintained at 26°C for 12 and 14/15 days, and used for the midgut and salivary gland

432   dissections, respectively. The midgut or salivary gland sporozoites were isolated into HC-04

433   complete culture medium (MEM without L-glutamine (Gibco) supplemented with F-12 Nutrient

434   Mix with L-glutamine (Gibco) in 1:1 ratio, 15 mM HEPES, 1.5 g/L NaHCO3, 2.5 mM additional

435   L-glutamine, 10% FCS) and kept on ice until further use.

Imaging flow cytometry of sporozoites

436

437   Isolated sporozoites were diluted in PBS/1% FCS to 3×10^6/mL and incubated for 30 min

438   at 4°C with 1 µg/mL recombinant IgGs, washed (16,000 x g, 4 min, 4°C) and incubated with Cy5-

439   conjugated anti-human IgG1 (0.4 µg/ml, DRFZ Core Facility, Berlin) for 30 min at 4°C. After

440   incubation with the secondary antibody, sporozoites were further incubated with propidium iodide

441   (20 µg/mL, Sigma Aldrich) for 5 min at room temperature as previously described (Costa et al.,

442   2018). Sporozoites were acquired after one wash in PBS using the ImageStreamX Mk II instrument

443   (Merck Millipore) with a 60X objective for 15-20 min per sample. The experiments were

444   performed in three replicates. To avoid a possible bias due to the variable pre-acquisition waiting

445   times on ice, the order of samples was swapped between the experimental replicates.

446   Quantification of propidium iodide staining was performed using the Intensity_MC_Ch04,

447   whereas mAb binding was quantified by Cy5-conjugated secondary antibody signal

448   Intensity_MC_Ch11. Single sporozoites were manually selected by brightfield images (Channel

449   9) and only live, propidium iodide-negative sporozoites were gated for mAbs binding efficiency

450   analysis (for gating strategy see Fig. S2). The analysis was performed with IDEAS 6.2 (Merck

451   Millipore). Raw data were exported as .txt files and represented in dot and density plots using

452   RStudio Version 1.1.453.

Pf sporozoite hepatocyte traversal assay

453

454   Pf traversal assays were performed as previously described (Triller et al., 2017). In brief,

455   the salivary gland sporozoites were isolated from mosquito thorax and treated with mAbs (100

456   µg/mL) for 30 min on ice. The sporozoite preparations were seeded on human hepatocytes (HC-

457   04; Sattabongkot et al., 2006) for 2 h at 37°C and 5% CO2 in the presence of dextran-rhodamine

458   (0.5 mg/mL) (Molecular Probes). mAb-untreated Pf sporozoites were used to measure the

459   maximum traversal capacity. Cells incubated only with uninfected mosquito thoracic material

460   were used as a background control. Cells were washed and fixed with 1% (v/v) formaldehyde in

461   PBS. Dextran positivity was detected by FACS LSR II instrument (BD Biosciences). Data analysis

462   was performed by background subtraction and normalization to the maximum traversal capacity

463   of mAb-untreated Pf sporozoites using FlowJo v.10.0.8 (Tree Star).

464   **Passive transfer of scFabs into mosquitoes**

465   1-2-day-old female *A. coluzzii* mosquitoes were injected on ice with 100 ng (285 µL) of scFab

466   diluted in PBS or with 285 µL PBS as an injection control. Two days later, mosquitoes were

467   infected with *P. falciparum* NF54 following the protocol described above. Mosquito heads were

468   carefully pulled off 14 days later and the attached salivary glands were collected and washed with

469   PBS. Dissected salivary glands were pooled for each group, homogenized and the freshly isolated

470   sporozoites were counted using a Malassez hemocytometer. The average number of sporozoites

471   per mosquito was calculated for each group.

472   **Enzyme-linked immunosorbent assay**

473   Antigen ELISA detHigh binding 384 well polystyrene plates (Corning) were coated with

474   recombinantly expressed PfCSP$_{71-104}$ comprising N-CSP at 50 ng/well overnight at 4°C. 1% BSA

475   in PBS was used for blocking the wells at RT. Binding of mAbs to N-CSP was determined by

476   incubating the coated plates with serially diluted mAb at 4.00, 1.00, 0.25, 0.06 µg/mL

477   concentrations. Bound mAb was detected using goat anti–human IgG-HRP (Jackson

478   ImmunoResearch) at 1:1,000 dilution in 1% BSA in PBS and One-step ABTS substrate (Roche).

479   Non-PfCSP reactive antibody, mGO53, was used as negative control (Wardemann et al., 2003).

480   Area under the curve (AUC) based on diluted antibody series was calculated using GraphPad

481   Prism 7.04 (GraphPad).

23

482   **Statistical analysis**

483   No samples were excluded from the analyses. Mosquitoes from the same batches were

484   randomly allocated to the experimental groups (age range: 1–2 days). The experimenters were not

485   blinded to the group allocation during the experiment and/or when assessing the outcome. Sample

486   sizes were chosen according to best practices in the field and previous experience (Costa et al.,

487   2018).

488   For Figures 3C and 4C, Mean Fluorescence Intensity (MFI) and standard error of the mean

489   (SEM) of the mAb-bound live sporozoites were first computed from the data. We then associated

490   an MFI and standard error to each treatment by computing the average MFI across the three

491   independent experiments and subsequently computing the standard deviation (STD) as STD =

492    $[(SEM_1^2 + SEM_2^2 + SEM_3^2)^{1/2}]/3$. The null hypothesis was that the MFIs of sporozoites bound by

493   the tested mAbs were not different. Due to the large sample sizes examined, a z-test was used to

494   compare the MFI of the three conditions, and the obtained p-values are summarized below with

495   significant p-values highlighted in green:

496

497
498

Fig. 3C	5D5	5D5Δg		Fig. 4C	5D5	5D5Δg
1210	$<10^{-4}$	$<10^{-4}$		1210	$<10^{-4}$	$<10^{-4}$
5D5	-	0.2		5D5	-	0.3
5D5Δg		-		5D5Δg		-

499

500   The combined *p*-values from the z-test were much smaller than the total sample size, which is

501   roughly 10^4. *p*-values much smaller than the inverse of the population size were therefore rounded

502   up to 10^{-4}.

503   For Figures 3D and 4D, sample sizes (*tot1*) and proportion of mAb-bound sporozoites per

504   experiments (*pos1*) for each independent experiment (N=3) are summarized below:

24

Fig. 3D	Exp 1		Exp 2		Exp 3	
	tot1	pos1	tot1	pos1	tot1	pos1
1710	806	0	589	1	1121	1
1210	266	223	447	401	138	112
5D5	545	176	487	82	1096	316
5D5Δg	592	95	665	69	653	81

Fig. 4D	Exp 1		Exp 2		Exp 3	
	tot1	pos1	tot1	pos1	tot1	pos1
1710	901	2	1987	1	1267	4
1210	222	219	681	675	837	831
5D5	262	67	728	229	1456	366
5D5Δg	471	72	738	97	1482	193

The null hypothesis was that the proportions of sporozoites bound by the tested mAbs were not different. Normality was verified and a z-test was used to compare the fractions of mAb-bound sporozoites. We first computed the fraction f of mAb-bound for each mosquito tissue, experiment and treatment as $f_i = \text{pos}_i / \text{tot}_i$. The fraction f can be considered as the probability that a sporozoite taken at random is bound by a certain mAb. The error associated to f is therefore given by $s(f) = \sqrt{f(1-f)/N}$, where N is the sample size given in the column $tot1$. Within each experiment, we used a two-sided z-test to test the null hypothesis that the fractions f associated to the tested mAbs were not different, resulting in six pairwise comparisons per experiment. The resulting p-values from the three independent experiments were combined using Fisher method and are summarized below with significant p-values highlighted in green:

Fig. 3D	1210	5D5	5D5Δg
1710	$<10^{-4}$	$<10^{-4}$	$<10^{-4}$
1210	-	$<10^{-4}$	$<10^{-4}$
5D5		-	$<10^{-4}$

Fig. 4D	1210	5D5	5D5Δg
1710	$<10^{-4}$	$<10^{-4}$	$<10^{-4}$
1210	-	$<10^{-4}$	$<10^{-4}$
5D5		-	$<10^{-4}$

For both Figures 3D and 4D, the fractions f organized from strong to weak are as follows: 1210, 5D5, 5D5Δg, 1710. The combined p-values computed with the Fisher method are much smaller than the total sample size, which is roughly 10^4. The reported p-values are therefore the inverse of the total sample size.

531   Statistical analysis in Figure 3E was performed using GraphPad Prism 8 (paired Friedman

532   test followed by Dunn's post-hoc test, paired values for mAb treatment per experiment) and p-

533   values below 0.05 were considered significant (*p < 0.05).

534   For Figure 4F, number of dissected mosquitoes and mean number of sporozoites per

535   mosquito in each independent experiment (N=6) are summarized below:

536

537

Exp	PBS	5D5	1710	1210
1	33	33	33	33
2	20	23	13	20
3	23	23	23	23
4	20	20	20	20
5	24	24	24	24
6	21	21	21	21

Numbers of dissected mosquitoes

Exp	PBS	5D5	1710	1210
1	34285	60612	46394	15510
2	22545	15058	10505	8803
3	7733	7304	13743	5333
4	6625	5000	4250	3750
5	811	1275	579	115
6	30095	19428	31047	14666

Mean number of sporozoites per mosquito

550   The null hypothesis was that the average number of sporozoites for each scFab and for each

551   experiment independently was not significantly different. To perform this test, we used the number

552   of oocysts per mosquito from the same experiments (data available upon request). We have

553   assumed that the number of oocysts per mosquito follows a negative binomial distribution with

554   average oocyst number M and shape parameter k:

$$\Pr\{X = m \mid k, M\} = \frac{\Gamma(m + k)}{\Gamma(k)\, m!} \left(\frac{k}{M + k}\right)^k \left(\frac{M}{M + k}\right)^m$$

558   that gives the probability that the number X of oocysts in one mosquito is equal to m, for $m =$

559     $0, 1, 2,$ etc. We determined the two parameters M and k using a Bayesian approach with the

560   Metropolis-Hastings algorithm and determined their MLE (code available upon request). The

561   estimates for k are given here:

562

	PBS	5D5	1710	1210
Exp				
1	1.15	1.07	1.37	0.97
2	0.33	0.14	0.36	0.42
3	33.3	2.44	1.76	1.37
4	0.43	0.22	0.32	0.52
5	0.47	0.38	0.56	0.36
6	0.43	0.26	0.39	0.27

Shape parameter k (MLE)

	PBS	5D5	1710	1210
Exp				
1	21	25	15	16
2	27	18	27	28
3	11	11	11	11
4	17	22	20	19
5	19	16	16	18
6	16	20	20	17

Numbers of dissected mosquitoes used for oocyst count to perform MLE estimates

569 We then assumed that the number of sporozoites was linearly proportional to the number of oocysts

570 (Vaughan et al., 1992; Stone et al., 2013; Miura et al., 2019). This allowed us to replace M (as

571 derived from oocysts distribution) in the negative binomial with the average sporozoite number as

572 given above. We used the MLE estimate of the shape parameter k and simulated 10,000

573 independent samples of mosquitoes of size given above. Each simulated sample is thus statistically

574 identical to those provided by the experimental data.

575 Finally, for each two treatments and for each pair of simulated samples, we tested the null

576 hypothesis that there is no difference between the treatments by random sampling while keeping

577 sample sizes as in the experimental data. We thus created a distribution of the difference between

578 the average number of sporozoites in the two treatments to be compared under this null

579 hypothesis. The comparison of this distribution with the difference in sporozoite numbers as

580 given by the experimental data produces the p-value listed below. The combined p-value using

581 the Fisher method and true from false positives were discriminated using the Benjamini-

582 Hochberg (BH) and the Benjamini-Liu (BL) methods at a false discovery rate $Q = 10^{-3}$.

583

584

trmt1	trmt2	exp1	exp2	exp3	exp4	exp5	exp6	Fisher	BH Q = 1e-3	BL
PBS	5D5	0.99	0.25	0.35	0.30	0.84	0.20	0.54	False	False
PBS	1710	0.91	0.14	0.99	0.19	0.21	0.53	0.45	False	False
PBS	1210	2e-3	0.07	0.02	0.12	0.01	0.09	8e-6	True	True
5D5	1710	0.13	0.34	0.99	0.39	0.06	0.81	0.29	False	False
5D5	1210	1e-4	0.22	0.08	0.30	0.01	0.31	1e-4	True	True
1710	1210	3e-4	0.36	1e-3	0.40	0.01	0.09	3e-6	True	True

Comparison between treatments across experiments, p-values and FDR analysis.

To check the consistency of this method, we simulated the sampled mosquito populations but

skipped the shuffling across the samples.

(Online) Supplemental Material

Supplemental materials include three tables and three figures. Supplemental tables: X-ray

crystallography data collection and refinement (Table S1), description of primers used to generate

mutant insert library for yeast display (Table S2), and PCR reactions and products for mutant insert

library construction (Table S3). Supplemental figures: Experimental details of fluorescence-

activated cell sorting of 5D5 IgG yeast display epitope mapping library and crystal structure

(Figure S1), gating strategy for imaging flow cytometry quantification of mAb binding to live Pf

sporozoites (Figure S2), and human mAbs against the PfCSP N-CSP identified from analysis of

the PfSPZ-CVac samples (Figure S3).

Author contributions

ET, GC, AW, RM, DO, SWS, IAW, HW, JPJ, EAL, conceived and designed the research; ET,

GC, AW, RM, DO, NCW, KP, AB, NW, TP performed the research; ET, GC, AW, RM, DO,

606   AV, SWS, IAW, NCW, PP, HW, JPJ, EAL, analyzed data; ET, GC, AW, HW, JPJ, EAL wrote

607   the paper with input from all authors.

References

627

628   1.   World Health Organization. 2018. World malaria report 2018.

629   https://www.who.int/malaria/publications/world-malaria-report-2018/report/en/ (accessed

630   June 6, 2019).

631   2.   Potocnjak, P., N. Yoshida, R.S. Nussenzweig, and V. Nussenzweig. 1980. Monovalent

632   fragments (Fab) of monoclonal antibodies to a sporozoite surface antigen (Pb44) protect mice

633   against malaria infection. *J. Exp. Med.* 151:1504–1513. doi:10.1084/jem.151.6.1504.

634   3.   Yoshida, N., R.S. Nussenzweig, P. Potocnjak, V. Nussenzweig, M. Aikawa. 1980.

635   Hybridoma produces protective antibodies directed against the sporozoite stage of malaria

636   parasite. *Science.* 207:71–73. doi:10.1126/science.6985745.

637   4.   Yoshida, N., P. Potocnjak, V. Nussenzweig, and R.S. Nussenzweig. 1981. Biosynthesis of

638   Pb44, the protective antigen of sporozoites of *Plasmodium berghei*. *J. Exp. Med.* 154:1225–

639   1236. doi:10.1084/jem.154.4.1225.

640   5.   Cochrane, A.H., F. Santoro, V. Nussenzweig, R.W. Gwadz, and R.S. Nussenzweig. 1982.

641   Monoclonal antibodies identify the protective antigens of sporozoites of *Plasmodium*

642   *knowlesi*. *Proc. Natl. Acad. Sci. USA*. 79:5651–5655. doi:10.1073/pnas.79.18.5651.

643   6.   RTS,S Clinical Trials Partnership. 2015. Efficacy and safety of RTS,S/AS01 malaria vaccine

644   with or without a booster dose in infants and children in Africa: final results of a phase 3,

645   individually randomised, controlled trial. *Lancet*. 386:31–45. doi:10.1016/S0140-

646   6736(15)60721-8.

647   7.   Julien, J.-P., and H. Wardemann. 2019. Antibodies against *Plasmodium falciparum* malaria

648   at the molecular level. *Nat. Rev. Immunol.* 19: 761-775. doi:10.1038/s41577-019-0209-5.

649   8.   Foquet, L., C.C. Hermsen, G. Van Gemert, E. Van Braeckel, K.E. Weening, R. Sauerwein, P.

650   Meuleman, and G. Leroux-roels. 2014. Vaccine-induced monoclonal antibodies targeting

651   circumsporozoite protein prevent *Plasmodium falciparum* infection. *J. Clin. Invest.* 124:140–

652   144. doi:10.1172/JCI70349.

653 9. Oyen, D., J.L. Torres, U. Wille-Reece, C.F. Ockenhouse, D. Emerling, J. Glanville, W.

654   Volkmuth, Y. Flores-Garcia, F. Zavala, A.B. Ward, C.R. King, and I.A. Wilson. 2017.

655   Structural basis for antibody recognition of the NANP repeats in *Plasmodium falciparum*

656   circumsporozoite protein. *Proc Natl Acad Sci USA*. 114:E10438–E10445.

657   doi:10.1073/pnas.1715812114.

658 10. Triller, G., S.W. Scally, G. Costa, M. Pissarev, C. Kreschel, A. Bosch, E. Marois, B.K. Sack,

659   R. Murugan, A.M. Salman, C.J. Janse, S.M. Khan, S.H.I. Kappe, A.A. Adegnika, B.

660   Mordmüller, E.A. Levashina, J.P. Julien, and H. Wardemann. 2017. Natural parasite

661   exposure induces protective human anti-malarial antibodies. *Immunity*. 47:1197-1209.e10.

662   doi:10.1016/j.immuni.2017.11.007.

663 11. Kisalu, N.K., A.H. Idris, C. Weidle, Y. Flores-Garcia, B.J. Flynn, B.K. Sack, S. Murphy, A.

664   Schön, E. Freire, J.R. Francica, A.B. Miller, J. Gregory, S. March, H.X. Liao, B.F. Haynes,

665   K. Wiehe, A.M. Trama, K.O. Saunders, M.A. Gladden, A. Monroe, M. Bonsignori, M.

666   Kanekiyo, A.K. Wheatley, A.B. McDermott, S.K. Farney, G.Y. Chuang, B. Zhang, N. Kc, S.

667   Chakravarty, P.D. Kwong, P. Sinnis, S.N. Bhatia, S.H.I. Kappe, B.K.L. Sim, S.L. Hoffman,

668   F. Zavala, M. Pancera, and R.A. Seder. 2018. A human monoclonal antibody prevents

669   malaria infection by targeting a new site of vulnerability on the parasite. *Nat. Med.* 24:408–

670   416. doi:10.1038/nm.4512.

671 12. Tan, J., B.K. Sack, D. Oyen, I. Zenklusen, L. Piccoli, S. Barbieri, M. Foglierini, C.S. Fregni,

672   J. Marcandalli, S. Jongo, S. Abdulla, L. Perez, G. Corradin, L. Varani, F. Sallusto, B.K.L.

673   Sim, S.L. Hoffman, S.H.I. Kappe, C. Daubenberger, I.A. Wilson, and A. Lanzavecchia.

674   2018. A public antibody lineage that potently inhibits malaria infection through dual binding

675   to the circumsporozoite protein. *Nat. Med.* 24:401–407. doi:10.1038/nm.4513.

676   13. Imkeller, K., S. Scally, A. Bosch, G. Pidelaserra Martí, G. Costa, G. Triller, R. Murugan, P.

677   Kremsner, S. Hoffman, B. Mordmüller, E. Levashina, J. Julien, and H. Wardemann. 2018.

678   Antihomotypic affinity maturation improves human B cell responses against a repetitive

679   epitope. *Science.* 360:1358–1362. doi:10.1126/science.aar5304.

680   14. Murugan, R., S.W. Scally, G. Costa, G. Mustafa, E. Thai, T. Decker, A. Bosch, K. Prieto,

681   E.A. Levashina, J.-P. Julien, and H. Wardemann. 2019. Evolution of protective human

682   antibodies against *Plasmodium falciparum* circumsporozoite protein repeat motifs. *bioRxiv.*

683   798769. doi:10.1101/798769.

684   15. Scally, S.W., R. Murugan, A. Bosch, G. Triller, G. Costa, B. Mordmüller, P.G. Kremsner,

685   B.K.L. Sim, S.L. Hoffman, E.A. Levashina, H. Wardemann, and J.P. Julien. 2018. Rare

686   PfCSP C-terminal antibodies induced by live sporozoite vaccination are ineffective against

687   malaria infection. *J. Exp. Med.* 215:63–75. doi:10.1084/jem.20170869.

688   16. Espinosa, D.A., G.M. Gutierrez, M. Rojas-Lopez, A.R. Noe, L. Shi, S.W. Tse, P. Sinnis, and

689   F. Zavala. 2015. Proteolytic cleavage of the *Plasmodium falciparum* circumsporozoite

690   protein is a target of protective antibodies. *J. Infect. Dis.* 212:1111–1119.

691   doi:10.1093/infdis/jiv154.

692   17. Herrera, R., C. Anderson, K. Kumar, A. Molina-Cruz, V. Nguyen, M. Burkhardt, K. Reiter,

693   R. Shimp, R.F. Howard, P. Srinivasan, M.J. Nold, D. Ragheb, L. Shi, M. DeCotiis, J. Aebig,

694   L. Lambert, K.M. Rausch, O. Muratova, A. Jin, S.G. Reed, P. Sinnis, C. Barillas-Mury, P.E.

695   Duffy, N.J. MacDonald, and D.L. Naruma. 2015. Reversible conformational change in the

696   *Plasmodium falciparum* circumsporozoite protein masks its adhesion domains. *Infect.*

697   *Immun.* 83:3771–3780. doi:10.1128/IAI.02676-14.

698   18. Dame, J.B., J.L. Williams, T.F. McCutchan, J.L. Weber, R.A. Wirtz, W.T. Hockmeyer, W.L.

699   Maloy, J.D. Haynes, I. Schneider, D. Roberts, G.S. Sanders, E.P. Reddy, C.L. Diggs, and

700   L.H. Miller. 1984. Structure of the gene encoding the immunodominant surface antigen on

701   the sporozoite of the human malaria parasite *Plasmodium falciparum*. *Science.* 225:593–599.

702   doi:10.1126/science.os-1.14.154.

703   19. Coppi, A., C. Pinzon-Ortiz, C. Hutter, and P. Sinnis. 2005. The *Plasmodium*

704   circumsporozoite protein is proteolytically processed during cell invasion. *J. Exp. Med.*

705   201:27–33. doi:10.1084/jem.20040989.

706   20. Drozdetskiy, A., C. Cole, J. Procter, and G.J. Barton. 2015. JPred4: a protein secondary

707   structure prediction server. *Nucleic Acids Res.* 43:W389–W394. doi:10.1093/nar/gkv332.

708   21. Baker, N.A., D. Sept, S. Joseph, M.J. Holst, and J.A. McCammon. 2001. Electrostatics of

709   nanosystems: application to microtubules and the ribosome. *Proc Natl Acad Sci USA*.

710   98:10037–10041. doi:10.1073/pnas.181342398.

711   22. Zhao, J., P. Bhanot, J. Hu, and Q. Wang. 2016. A comprehensive analysis of *Plasmodium*

712   circumsporozoite protein binding to hepatocytes. *PLoS One*. 11:e0161607.

713   doi:10.1371/journal.pone.0161607.

714   23. Varki, A., R.D. Cummings, M. Aebi, N.H. Packer, P.H. Seeberger, J.D. Esko, P. Stanley, G.

715   Hart, A. Darvill, T. Kinoshita, J.J. Prestegard, R.L. Schnaar, H.H. Freeze, J.D. Marth, C.R.

716   Bertozzi, M.E. Etzler, M. Frank, J.F.G. Vliegenthart, T. Lütteke, S. Perez, E. Bolton, P.

717   Rudd, J. Paulson, M. Kanehisa, P. Toukach, K.F. Aoki-Kinoshita, A. Dell, H. Narimatsu, W.

718   York, N. Taniguchi, and S. Kornfeld. 2015. Symbol nomenclature for graphical

34

719   representations of glycans. *Glycobiology*. 25:1323–1324. doi:10.1093/glycob/cwv091.

720   24. Menard, R., A.A. Sultan, C. Cortest, R. Ahszulert, M.R. van Dijk, C.J. Janse, A.P. Waters,

721   R.S. Nussenzweig, and V. Nussenzweig. 1997. Circumsporozoite protein is required for

722   development of malaria sporozoites in mosquitoes. *Nature*. 385:336–340.

723   doi:10.1038/385336a0.

724   25. Murugan, R., L. Buchauer, G. Triller, C. Kreschel, G. Costa, G. Pidelaserra Martí, K.

725   Imkeller, C.E. Busse, S. Chakravarty, B.K.L. Sim, S.L. Hoffman, E.A. Levashina, P.G.

726   Kremsner, B. Mordmüller, T. Höfer, and H. Wardemann. 2018. Clonal selection drives

727   protective memory B cell responses in controlled human malaria infection. *Sci. Immunol.*

728   3:eaap8029. doi:10.1126/sciimmunol.aap8029.

729   26. Van Blarcom, T., A. Rossi, D. Foletti, P. Sundar, S. Pitts, C. Bee, J. Melton Witt, Z. Melton,

730   A. Hasa-Moreno, L. Shaughnessy, D. Telman, L. Zhao, W.L. Cheung, J. Berka, W. Zhai, P.

731   Strop, J. Chaparro-Riggers, D.L. Shelton, J. Pons, and A. Rajpal. 2015. Precise and efficient

732   antibody epitope determination through library design, yeast display and next-generation

733   sequencing. *J. Mol. Biol.* 427:1513–1534. doi:10.1016/j.jmb.2014.09.020.

734   27. Chao, G., W.L. Lau, B.J. Hackel, S.L. Sazinsky, S.M. Lippow, and K.D. Wittrup. 2006.

735   Isolating and engineering human antibodies using yeast surface display. *Nat. Protoc.* 1:755–

736   768. doi:10.1038/nprot.2006.94.

737   28. Benatuil, L., J.M. Perez, J. Belk, and C.M. Hsieh. 2010. An improved yeast transformation

738   method for the generation of very large human antibody libraries. *Protein Eng. Des. Sel.*

739   23:155–159. doi:10.1093/protein/gzq002.

740   29. Ekiert, D.C., R.H.E. Friesen, G. Bhabha, T. Kwaks, M. Jongeneelen, W. Yu, C. Ophorst, F.

741   Cox, H.J.W.M. Korse, B. Brandenburg, R. Vogels, J.P.J. Brakenhoff, R. Kompier, M.H.

742   Koldijk, L.A.H.M. Cornelissen, L.L.M. Poon, M. Peiris, W. Koudstaal, I.A. Wilson, and J.

743   Goudsmit. 2011. A highly conserved neutralizing epitope on group 2 influenza A viruses.

744   *Science.* 333:843–850. doi:10.1126/science.1204839.

745 30. Mordmüller, B., G. Surat, H. Lagler, S. Chakravarty, A.S. Ishizuka, A. Lalremruata, M.

746   Gmeiner, J.J. Campo, M. Esen, A.J. Ruben, J. Held, C.L. Calle, J.B. Mengue, T. Gebru, J.

747   Ibáñez, M. Sulyok, E.R. James, P.F. Billingsley, K. Natasha, A. Manoj, T. Murshedkar, A.

748   Gunasekera, A.G. Eappen, T. Li, R.E. Stafford, M. Li, P.L. Felgner, R.A. Seder, T.L. Richie,

749   B.K.L. Sim, S.L. Hoffman, and P.G. Kremsner. 2017. Sterile protection against human

750   malaria by chemoattenuated PfSPZ vaccine. *Nature*. 542:445–449. doi:10.1038/nature21060.

751 31. Cock, P.J.A., T. Antao, J.T. Chang, B.A. Chapman, C.J. Cox, A. Dalke, I. Friedberg, T.

752   Hamelryck, F. Kauff, B. Wilczynski, and M.J.L. De Hoon. 2009. Biopython: freely available

753   Python tools for computational molecular biology and bioinformatics. *Bioinformatics*.

754   25:1422–1423. doi:10.1093/bioinformatics/btp163.

755 32. Kabsch, W. 2010. XDS. *Acta Crystallogr. D Biol. Crystallogr.* 66:125–132. https://doi .org

756   /10 .1107 /S0907444909047337

757 33. McCoy, A.J., R.W. Grosse-Kunstleve, P.D. Adams, M.D. Winn, L.C. Storoni, and R.J. Read.

758   2007. Phaser crystallographic software. *J. Appl. Cryst.* 40:658–674. https ://doi .org /10 .1107

759   /S0021889807021206

760 34. Adams, P.D., P.V. Afonine, G. Bunkóczi, V.B. Chen, I.W. Davis, N. Echols, J.J. Headd,

761   L.W. Hung, G.J. Kapral, R.W. Grosse-Kunstleve, et al. 2010. PHE NIX: a comprehensive

762   Python-based system for macromolecular structure solution. *Acta Crystallogr. D Biol.*

763   *Crystallogr.* 66:213–221. https ://doi .org /10 .1107 /S0907444909052925

764   35. Emsley, P., B. Lohkamp, W.G. Scott, and K. Cowtan. 2010. Features and development of

765   Coot. *Acta Crystallogr. D Biol. Crystallogr.* 66:486–501. https ://doi .org /10 .1107

766   /S0907444910007493

767   36. Costa, G., M. Gildenhard, M. Eldering, R.L. Lindquist, A.E. Hauser, R. Sauerwein, C.

768   Goosmann, V. Brinkmann, P. Carrillo-Bustamante, and E.A. Levashina. 2018. Non-

769   competitive resource exploitation within mosquito shapes within-host malaria infectivity and

770   virulence. *Nat. Commun.* 9:1–11. doi:10.1038/s41467-018-05893-z.

771   37. Sattabongkot, J., N. Yimamnuaychoke, S. Leelaudomlipi, M. Rasameesoraj, R. Jenwithisuk,

772   R.E. Coleman, R. Udomsangpetch, L. Cui, and T.G. Brewer. 2006. Establishment of a human

773   hepatocyte line that supports in vitro development of the exo-erythrocytic stages of the

774   malaria parasites *Plasmodium falciparum* and P. vivax. *Am. J. Trop. Med. Hyg.* 74:708–715.

775   doi:10.4269/ajtmh.2006.74.708.

776   38. Wardemann, H., S. Yurasov, A. Schaefer, J.W. Young, E. Meffre, and M.C. Nussenzweig.

777   2003. Predominant autoantibody production by early human B cell precursors. *Science.*

778   301:1374–1377. doi:10.1126/science.1086907.

779   39. Vaughan, J.A., B.H. Noden, and J.C. Beier. 1992. Population dynamics of *Plasmodium*

780   *falciparum* sporogony in laboratory-infected *Anopheles gambiae*. *J. Parasitol.* 78:716–724.

781   40. Stone, W.J.R., M. Eldering, G.-J. Van Gemert, K.H.W. Lanke, L. Grignard, M.G. Van De

782   Vegte-Bolmer, R. Siebelink-Stoter, W. Graumans, W.F.G. Roeffen, C.J. Drakeley, R.W.

783   Sauerwein, and T. Bousema. 2013. The relevance and applicability of oocyst prevalence as a

784   read-out for mosquito feeding assays. *Sci. Rep.* 3:1–8. doi:10.1038/srep03418.

785   41. Miura, K., B.J. Swihart, B. Deng, L. Zhou, T.P. Pham, A. Diouf, M.P. Fay, and C.A. Long.

786   2019. Strong concordance between percent inhibition in oocyst and sporozoite intensities in a

787   *Plasmodium falciparum* standard membrane-feeding assay. *Parasit Vectors*. 12: 206.

788   doi:10.1186/s13071-019-3470-3.